journal

J. Am. Ceram. Soc., 92 [10] 2311–2318 (2009)
DOI: 10.1111/j.1551-2916.2009.03224.x

Proofs of the Coexistence of Two Magnetic Contributions in Pure and Doped $CaCu_3Ti_4O_{12}$ Giant Dielectric Constant Ceramics

José Francisco Fernández,[†,‡] Pilar Leret,[‡] Juan José Romero,[‡] José de Frutos,[§] Miguel Ángel de la Rubia,[‡,§] María Soledad Martín-González,[¶] José Luis Costa-Krämer,[¶,‖] José Luis García Fierro,[**] Adrián Quesada,[††,‡‡] and Miguel Ángel García[‡]

[‡]Electroceramic Department, Instituto de Cerámica y Vidrio, CSIC, 28049 Madrid, Spain

[§]ETSI Telecomunicación, Universidad Politécnica de Madrid, 28040 Madrid, Spain

[¶]Instituto de Microelectrónica de Madrid, CSIC, Tres Cantos, 28760 Madrid, Spain

[‖]Tate Laboratory of Physics, University of Minnesota, Minneapolis, Minnesota 55455

[**]Instituto de Catálisis y Petroleoquímica, CSIC, 28049 Madrid, Spain

[††]Dpto. Física de Materiales e Instituto de Magnetismo Aplicado, Universidad Complutense de Madrid, 28240 Madrid, Spain

[‡‡]National Center for Electron Microscopy, Lawrence Berkeley National Laboratory, Berkeley, California 94720

Fe^{3+}- or Nb^{5+}-doped $CaCu_3Ti_4O_{12}$ (CCTO) ceramics show higher values of both room-temperature (RT) grain conductivity and dielectric constant than undoped ceramics. Microstructural and structural characterization combined with magnetic properties reveal the coexistence of two components that seem relevant for the dielectric behavior of the material. The grain possesses a nanostructure characterized by layered domains with thicknesses <80 nm. The formation of the layered domains is associated with the evidence of different chemical states as Cu^{2+}/Cu^{+} and Ti^{4+}/Ti^{3+} that are present in the material. The magnetic contribution is related to two coupled effects: the antiferromagnetic (AFM) response with $T_N = 25$ K ascribed to Cu^{2+}, and a paramagnetic-like contribution attributed to Ti^{3+} cations. The coexistence of two coupled magnetic contributions could explain the proposed unusual coupling of the AFM Cu^{2+} superexchange interaction through the nonmagnetic Ti^{4+} rather than via the usual oxygen coupling. The lower the paramagnetic-like contribution at RT, the larger the conductivity and the dielectric constant of the material are. Below 150 K, the increase of the paramagnetic-like contribution is correlated with the low transition temperature of the CCTO.

I. Introduction

THE giant dielectric properties of $CaCu_3Ti_4O_{12}$ (CCTO), $\sim 3.5 \times 10^5$ for single-crystal[1] and $\sim 2.5 \times 10^5$ for ceramics,[2] have recently attracted great interest because they present a weak dependence on temperature and frequency. Therefore, this material seems promising for low-frequency microelectronic applications like decoupling capacitors. The CCTO has a distorted, complex cubic perovskite ABO_3-related structure with a large unit cell $a = 7.4$ Å.[2,3] The Cu cations are bonded to four oxygens in a square planar configuration on the A sites, causing the tilting of the TiO_6 octahedron.

Subramanian *et al.*[3] were the first to report large dielectric constants ($\sim 10^4$) in $ACu_3Ti_4O_{12}$-like compositions. Since then many works have appeared, but the origin of the giant dielectric response is still unclear. Several theories have been proposed, and one of the most widely accepted, put forward by Adams *et al.*,[2] is the internal boundary layer capacitor (IBLC). This model states that the dielectric behavior of CCTO does not come from intrinsic or from space charge polarization mechanisms, but from heterogeneities of the ceramic structure.[4,5] Stoichiometry has also been demonstrated to play a crucial role in obtaining giant permittivity values.[6] Any off stoichiometry results in the decrease of the low-frequency dielectric permittivity values. In order to understand the effect of stoichiometry, some dopants have been introduced into the CCTO structure. The B site doping with donors like Nb^{5+} or acceptors like Fe^{3+} cations has been reported to decrease the value of the dielectric plateau due to an increase in grain boundary layer thickness, resulting in a lower grain boundary capacitance.[7] Fe^{3+}- or Nb^{5+}-doped CCTO ceramics show a microstructure with homogeneous grain size <60 μm that contrasts with the large grains >100 μm of the undoped samples.[8] Capsoni *et al.*[9] showed that the dielectric constant can be increased by up to two orders of magnitude when substituting the Ti^{4+} cations by Fe^{3+}, Co^{2+}, or Ni^{2+}. They suggested, based on the IBLC model, that the residual CuO phase and grain boundary effects are responsible for this enhancement. The Nb^{5+} substitution for Ti^{4+} in CCTO was achieved in a limited range without secondary phase formation, and the dielectric constant increased up to $\sim 4.2 \times 10^5$.[10] While the grain (bulk) resistivity remains unchanged with Nb^{5+} substitution, the grain boundary resistivity is significantly reduced even though the grain size decreases, in contrast to the results shown in Grubbs *et al.*[7] This fact supports the improvement of the giant dielectric constant through the IBLC mechanism.

The analysis of the conductivity in ceramic CCTO reveals that it consists of *n*-type semiconducting grains with two kinds of insulating barrier layers: domain boundaries and grain boundaries.[11] The origin of this *n*-type behavior in CCTO remains controversial, and seems to be related to the presence of Ti^{3+} (d^1) due to the partial reduction of Ti^{4+} (d^0) associated with oxygen loss.[4] Li *et al.*[12], based on the high-temperature instability measurements, suggest that Cu^{2+} is reduced to Cu^{1+} by charge compensation and that Ti cations slightly occupy A sites, but this mechanism has not been proved yet. On cooling, the

X. M. Chen—contributing editor

Manuscript No. 25764. Received January 18, 2009; approved May 23, 2009.
This work was supported by the CSIC project PIF MAGIN and by CICYT project MAT2007-66845-C02-01.
[†]Author to whom correspondence should be addressed. e-mail: jfernandez@icv.csic.es

reoxidation of Cu^{1+} to Cu^{2+} promotes the appearance of Ti^{3+}. However, it has been found that bulk conductivity shows no significant variations when CCTO is treated under reducing or oxidizing atmospheres,[4] and the conduction mechanism has then been proposed to be related to a hole-doping conduction between Cu^{2+} and Cu^{3+}.[9]

CCTO exhibits an antiferromagnetic (AFM) transition at 25 K.[13] The AFM has been explained in terms of a double primitive cell, in which each Cu^{2+}–Cu^{2+} nearest-neighbor pair has antiparallel spins.[14] The Cu^{2+} superexchange interaction that leads to the AFM ordering has been suggested to occur[15] through the nonmagnetic Ti^{4+} ions located at the B positions of the perovskite rather than via the usual oxygen path. Fe^{3+} substitution on the Ti^{4+} B site should affect the AFM transition and results in a decrease of the Neel temperature, T_N.[7] In CCTO, the Cu^{2+} ions have an unusual, triply degenerate T_{2g} ground state, leading to a strong coupling between the crystallographic and magnetic substructures.[11] This strong coupling has been observed in the low-temperature dielectric anomaly associated with the onset of AFM order below 24 K.[7] However, T_N does not change when single-crystal CCTO is annealed in argon, suggesting two possibilities[16]: (i) some Cu^{2+} ions, $S = 1/2$, were missing; or (ii) the presence of oxygen vacancies transforms some of the Cu^{2+} ions into nonmagnetic Cu^{1+} and some of the Ti^{4+} ions into magnetic Ti^{3+} with $S = 1/2$. The low Curie-temperature tail that may be attributed to Ti^{3+} supports the second hypothesis. Pires *et al.*[16] assigned a contribution to the Ti^{3+} centers induced by the presence of oxygen vacancies in the intrinsic dielectric constant of CCTO materials, while the magnetic exchange interactions were not affected by this oxygen stoichiometry. Recently, Ni and Chen[17] reported, using XPS techniques, the presence of a polar arrangement of electrons in Cu^{+}/Cu^{2+} and Ti^{3+}/Ti^{4+} mixed valence states, in CCTO ceramics.

In this framework, an AFM transition occurs at a lower temperature than the dielectric region of interest, making the coupling between magnetic and dielectric properties very limited for possible applications. However, the presence of magnetic Ti^{3+} and its correlation with the giant permittivity is of great interest. By local spin density approximation, a field-induced AFM–FM transition is predicted in CCTO at a low temperature.[18] Moreover, a light-induced AFM–FM transition is also possible in the presence of a magnetic field, because CCTO has a metastable ferromagnetic and semiconducting state, according to spin-polarized and fixed-spin-moment methods.[18]

Despite the tremendous effort and large number of publications aiming to reveal the unusual properties of CCTO materials, several properties are still imprecisely determined, explanations are controversial, and experiments are not conclusive. This work studies undoped and doped CCTO ceramics, and correlates magnetic properties with the oxidation states of the Ti and Cu cations in the perovskite structure.

II. Experimental Procedure

Stoichiometric undoped samples of CCTO, acceptor-doped samples with 0.3 and 1 wt% cations of Fe^{3+} substituting Ti^{4+} cations (CCTOF03 and CCTOF, respectively), and donor-doped samples with 1 wt% cations of Nb^{5+} substituting Ti^{4+} cations (CCTON) were prepared by a conventional ceramic route. The analytical grade $CaCO_3$ (99.95%, Aldrich, St. Louis, MO), TiO_2 (99.5%, Merck, Darmstadt, Germany), CuO (99.9%, Aldrich), Nb_2O_5 (99.9%, Fluka, St. Louis, MO), and Fe_2O_3 (99.5%, Aldrich) powders were mixed for 2 h by attrition milling with 1.2 mm zirconia balls using deionized water as the liquid medium and 0.2 wt% of Dolapix C64 (Zschimmer & Schwarz, Villarreal, Spain) as dispersant. The milled powders were dried and sieved through a 100 μm nylon mesh. The powders were calcined at 1173 K for 12 h, and then attrition-milled again for 3 h. XRD of the synthesized powders showed a single perovskite phase without traces of secondary phases. Powders were dried and sieved through a 63 μm nylon mesh. Pellets of 8 mm in diameter and 1.3 mm in thickness were uniaxially pressed at 200 MPa and sintered in air at 1373 K for 32 h, with heating and cooling rates of 3 K/min. All samples show a density over 95% of the theoretical density. During handling, in both processing and characterization steps, polymer-based tools were used in order to avoid contamination by magnetic impurities.[19]

X-ray diffraction analyses were performed using $CuK\alpha_1$ radiation and a Ni filter (Siemens D5000, Erlangen, Germany). Microstructural features were observed by FESEM (Hitachi S-4700, Tokyo, Japan) and atomic force microscopy (model SOLVER PRO SPM, NT-MDT, Moscow, Russia). Polished disks were electroded with silver paint. The room-temperature (RT) dielectric properties were measured in an impedance analyzer (Agilent 4295A, Palo Alto, CA) at an oscillation voltage of 100 mV. Impedance spectroscopy measurements were performed in the frequency range of 10^2–10^7 Hz. Magnetic characterization was performed in a vibrating sample magnetometer (Quantum Design PPMS-VSM, San Diego, CA) in the temperature range of 5–300 K under an applied field of 20 kOe. Photoelectron spectra (XPS; VG ESCALAB 200R spectrometer, Thermo Scientific, Waltham, MA) were acquired with an $AlK\alpha$ X-ray source (1486.6 eV). Kinetic energies of the photoelectrons of interest were measured using a hemispherical electron analyzer operating in the constant pass energy mode. The base pressure along the analysis was maintained below 5.10^{-9} mbar. Before analysis, the samples were cleaned by ion-bombardment with an Ar^+ beam (2 kV) for 2 min. The XPS data were signal-averaged and taken in increments of 0.1 eV with dwelling times of 30 ms. Binding energies were calibrated relative to the C 1*s* peak from residual carbon contamination of the samples at 284.8 eV. High-resolution spectral envelopes were obtained by curve fitting synthetic peak components using the software package XPS peak. Raw data were used with no preliminary smoothing. Symmetric Gaussian–Lorentzian product functions were used to approximate line shapes of the fitting components.

III. Results and Discussion

(1) Dielectric Constant, Resistivity, and Microstructure

Table I summarizes data of the dielectric constant at 1 kHz and RT and the resistivity values at RT and 100 K of the prepared samples. The sample resistivity was considered as the intercept of the grain boundary semicircle with the real part of the impedance. Doped samples show larger dielectric constant values than undoped ones. The largest dielectric constant value is obtained for 1 wt% Fe-doped samples (2.8×10^5). The undoped ceramic shows an almost three orders of magnitude larger grain resistivity at RT than the doped samples, together with a weaker dependence with the temperature. Data from Table I are consistent with previous literature data[9,20,21] and account for the reproducibility of the doping effect. The larger dielectric constants are associated with lower RT resistivity in the doped samples. At 100 K, the resistivity of doped samples increased markedly. Below the temperature of 150 K, Sun *et al.*[22] established that the grain resistance increases quickly with the decrease of temperature and becomes large enough to make the IBLC capacitors' effect weaken, until it disappears. This provokes the steep decrease of the dielectric constant at this temperature.

Table I. Different Parameters of the CCTO Samples Studied in This Work (Average Grain Size, *d*, Determined from Microstructures of Leret *et al.*[8])

Sample	ε'_{RT} (at 1 kHz)	ρ_{RT} ($\Omega \cdot$ cm)	$\rho_{100\ K}$ ($\Omega \cdot$ cm)	d (μm)	t_B (nm)
CCTO	6800	$3.5\ 10^6$	$6.3\ 10^6$	133 ± 26	480
CCTON	129 500	$3.4\ 10^3$	$1.5\ 10^8$	23 ± 8	5
CCTOF03	146 750	$2.7\ 10^3$	$3.5\ 10^{10}$	37 ± 7	6
CCTOF	284 200	$1.0\ 10^4$	$8.6\ 10^8$	52 ± 9	5

The resistivity behavior of undoped CCTO prepared by the sol–gel process[22] was more similar to that of the doped samples than to the undoped ones in this study. In addition, the dielectric constant was considerably higher in the sol–gel-processed samples. This different behavior can be explained in terms of the barrier width (t_B), as given by[20] $\varepsilon' = \varepsilon_B(d/t_B)$, where ε_B is the dielectric constant of the barrier material and d the grain size. The t_B value for high-dielectric-constant, pure CCTO sol–gel samples[22] was $\sim$45 nm. Marchin *et al.*[23] found that $t_B < 10$ nm leads to a dielectric constant $> 5 \times 10^5$ at 1 kHz in undoped, soft chemistry processed CCTO with an excess of CuO. In the present work, the calculated t_B is $\sim$500 nm for undoped samples, while for the doped ones the values are $t_B < 10$ nm. Among others, different explanations are the presence of internal domains[24] or the polar arrangement of electrons on the mixed valence state of Cu^{2+}/Cu^{1+} and Ti^{4+}/Ti^{3+} pairs, as proposed recently.[17] More recently, Bueno *et al.*[25] proposed a model based on the presence of polaron electronic defects associated with stacking faults on CCTO. These polarons show a preferential conduction direction parallel to the stacking fault, creating nano-size barriers, which give rise to a nano-barrier layer capacitance model, working similarly to IBLC and concomitantly with it.

A very interesting feature of undoped samples is the appearance, in thermal etched samples, of a subgrain microstructure that might be considered as domain boundaries, and will be named hereafter as layered domains. The nature of these layered domains is still unclear, but it could be related to structurally different regions separated by stacking faults, or cation disorder regions inside single grains, as the ones previously observed by Wu *et al.*[26] on TEM images of both single-crystals and ceramics. These structural regions have been suggested to be on the origin of other types of disordered domains (bump domains and terrace-ledge domains) observed on CCTO ceramics.[11] Figure 1(a) shows the different orientation of layered domains in two adjacent grains, revealed on the polished surface of the sample after thermal etching. In this figure it is also possible to observe a recrystallization of the CuO-rich secondary phase (determined by EDS), which forms a liquid on the intergranular space. This phase was not observed in XRD experiments because the crystals are too small to be detected by that technique.

Thermal etching is the most straightforward method of revealing microstructures in ceramics.[27] It is based on the fact that upon heating a polycrystalline solid to a temperature T in the presence of a vapor or liquid phase in thermodynamic equilibrium with the solid, grooves appear at the grain boundaries as a result of material transfer diffusion mechanisms (surface and volume diffusion and condensation evaporation). The thermal etching treatment at 1233 K for 10 min is considerably shorter than others previously reported to reveal domain structures in CCTO.[11] The temperature used in the thermal etching treatment is higher than the liquid temperature of the grain boundary CuO-rich phase. In the presence of this liquid, the surface diffusion of Cu cations is from the origin of the recrystallization phenomenon that produces the subgrain structure. This subgrain structure is not observed in the doped samples because the low amount of CuO-rich secondary phase does not form any liquid that is able to decorate the grain boundaries.

Figure 1(b) shows an atomic force microscopic image of the detailed microstructure of the layered domains, showing an average domain thickness of $\sim$40 nm, although values up to 80 nm are observed. Particularly interesting is the fact that the domains cross the whole grain and the presence of porosity does not seem to affect the layered structure. Chung[28] found, by TEM observation, the presence of orientational domains in CCTO samples, but an ordered pattern was not observed.

Because the layered domain boundaries are revealed only in thermally etched samples and thus could be attributed to the thermal treatment preparation artifacts, it is necessary to find more evidences of their presence. For this reason, the different ceramic samples were dry-milled for 5 min in a nylon milling jar using yttrium-stabilized zircona balls of 2 mm in diameter. As an example, in Fig. 2 we show the morphology of the milled powders of sample CCTOF. For other samples the results are very similar. The powder consists of large particles with the typical fracture surfaces of brittle solids, as ceramics are, and layered small particles. It is difficult to determine if the large particles are thin enough, but the layered small ones possess an estimated thickness of well below 100 nm, in agreement with the thickness previously determined by AFM for the subgrain domains. It is quite unexpected that fragile ceramics with a cubic structure could be transformed into a layered powder, suggesting that the observed small particles reveal the presence of domains in the doped CCTO grains.

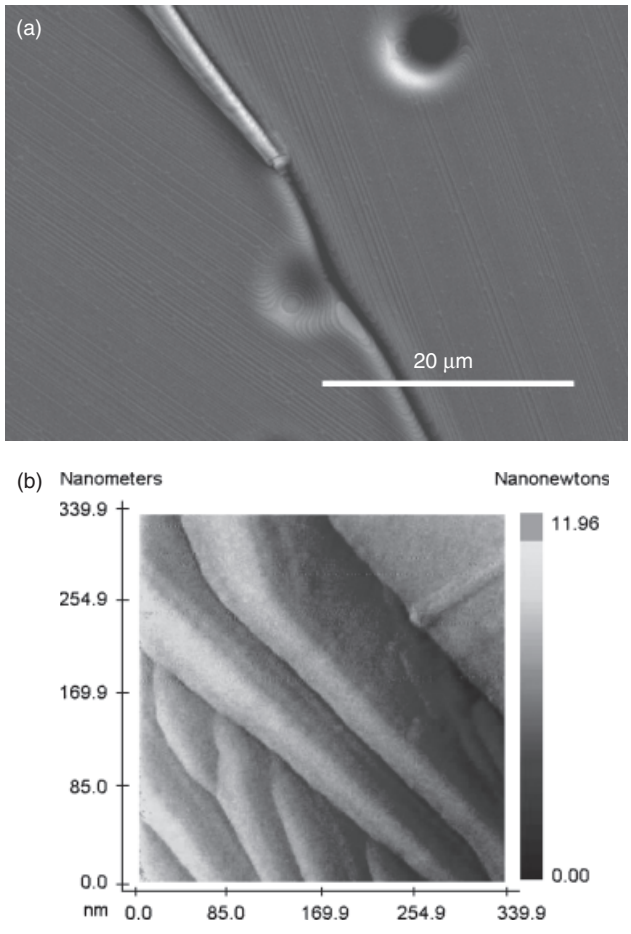

Fig. 1. (a) FESEM micrograph and (b) (color online) atomic force microscope image of an undoped CCTO ceramic.

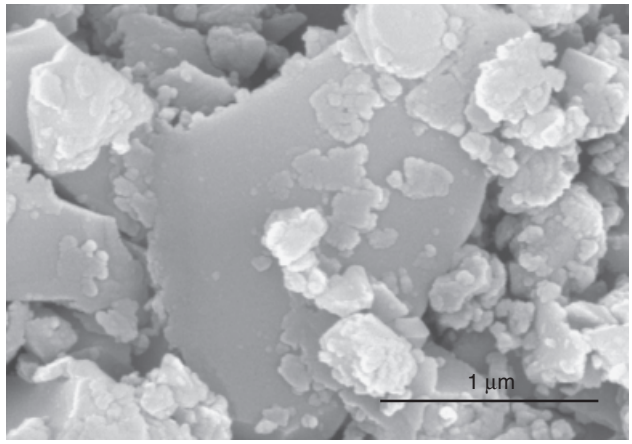

Fig. 2. FESEM micrograph of a milled CCTOF ceramic.

(2) Structure

XRD patterns (not shown here) correspond to a pure well-crystallized perovskite phase that could be indexed as a body-centered cubic perovskite-related structure of spatial group *Im*3, according to ICSD 032002.[3] The calculated *a* lattice parameters of the perovskite phase for the different materials were 7.394±0.007 Å for CCTO, 7.399±0.002 Å for CCTOF03, 7.402±0.002 Å for CCTOF, and 7.405±0.002 Å for CCTON, which are in good agreement with the reported RT lattice constant of CCTO, 7.391 Å.[3] The small differences observed were not evident enough to verify the incorporation of the dopant cations into the crystalline lattice. It is interesting to note that both dopants show a tendency to increase the lattice parameter, in disagreement with the ionic radius of the dopant cations.

Figures 3–7 show the core-level XPS spectra for undoped and doped ceramics. For comparison purposes, the XPS analysis of CCTOF milled as a powder and exposed to air (hereafter CCOTFp) is also shown. Figure 3 corresponds to the Ti 2*p* peak. The presence of three components, octahedral Ti^{4+} (457.9 eV), surface Ti^{4+} (459.4 eV), and Ti^{3+} (456.6 eV), are detected in CCTO and CCTOF. The amount of Ti^{3+} is almost negligible when the sample is doped with Nb^{5+} because of its oxidative nature. When the layered domains are exposed to air in the milled powders, the amount of reduced titanium increases and the surface Ti^{4+} decreases. The presence of Ti^{3+} must greatly distort the crystal because of the differences in ionic radius with Ti^{4+} and must be accompanied by the creation of oxygen vacancies and the formation of Ti^{3+}–O–Ti^{4+} bonds.[29]

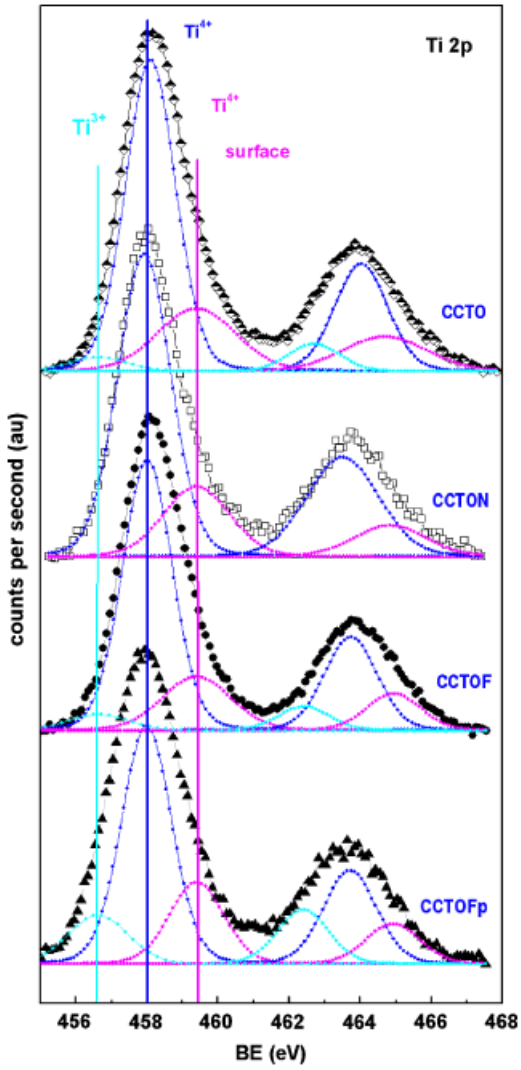

Fig. 3. Photoemission spectroscopy of Ti $2p_{3/2}$ core level for CCTO-based ceramics.

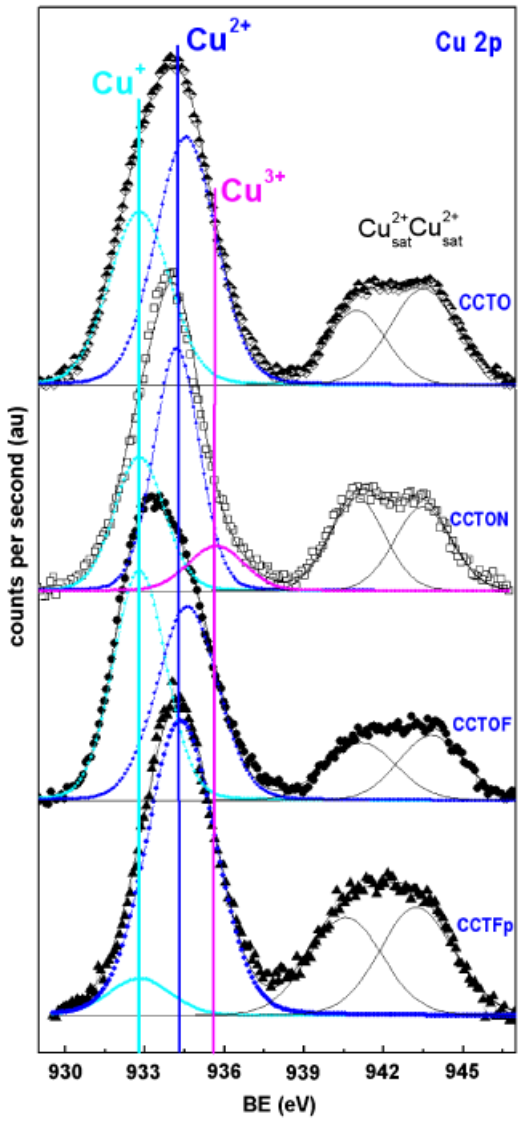

Fig. 4. Photoemission spectroscopy of the Cu $2p_{3/2}$ core level for CCTO-based ceramics.

In the case of the Cu 2*p* peak, as shown in Fig. 4, different oxidation states are also found. The main peak is the Cu^{2+} (934.4 eV) and a small contribution of Cu^{1+} or Cu^0 appears (both at 932.8 eV).[30,31] The presence of Cu^{1+}/Cu^0 is also minimum in the case of CCTON, but Cu^{3+} appears (935.1 eV), confirming the oxidation effect of the donor dopant cation. The presence of Cu^{3+} could support the proposed conduction mechanism via the hole hopping between Cu^{2+} and Cu^{3+}.[9] The amount of reduced Cu^{1+}/Cu^0 is higher than the amount of Cu^{2+} in CCTOF. For CCTOFp, the air exposure of the powders during milling favors the reoxidation of the surface copper cations, in contrast with the higher presence of reduced Ti cations.

In order to determine if the reduced copper is Cu^{1+} or Cu^0, the Cu_{LMM} Auger peaks were recorded and the spectra are shown in Fig. 5. The analysis establishes the reduced state of copper as Cu^{1+} (337 eV), discarding the presence of Cu^0 (335 eV). Cu^{2+} and Cu^{1+} are, respectively, the main oxidation states in CCTON and CCTOF. CCTO presents both Cu^{2+} and Cu^{1+}. The oxidation process of CCTOFp is confirmed, but the presence of a residual amount of Cu^{1+} is a clear indication of such an oxidation state even in milled powders. Note that XPS analysis only covers a few atomic layers from the surface, and thus the above results show that the surface copper cations exposed to air are more sensible to oxidation in the powders than in the bulk material.

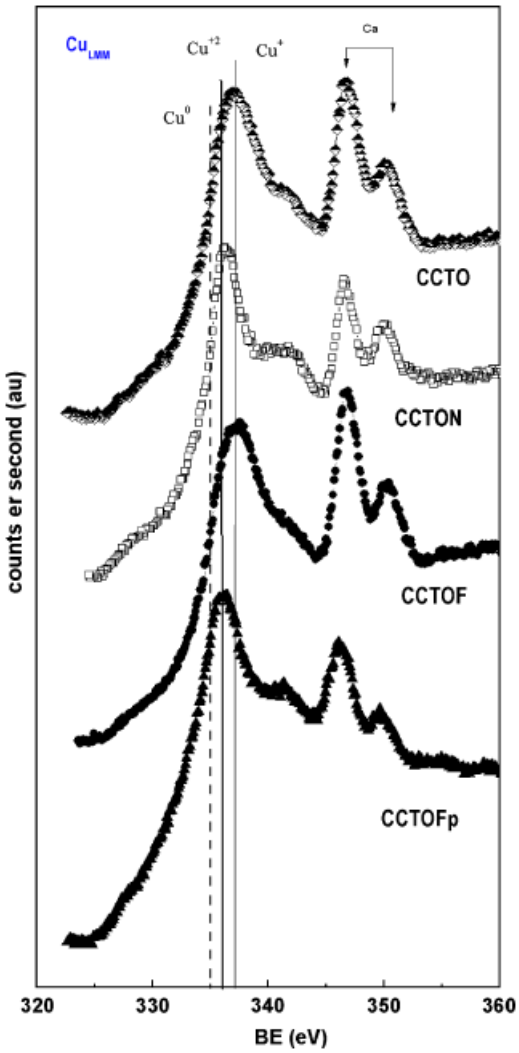

Fig. 5. Photoemission spectroscopy of the Cu_{LMM} core level for CCTO-based ceramics.

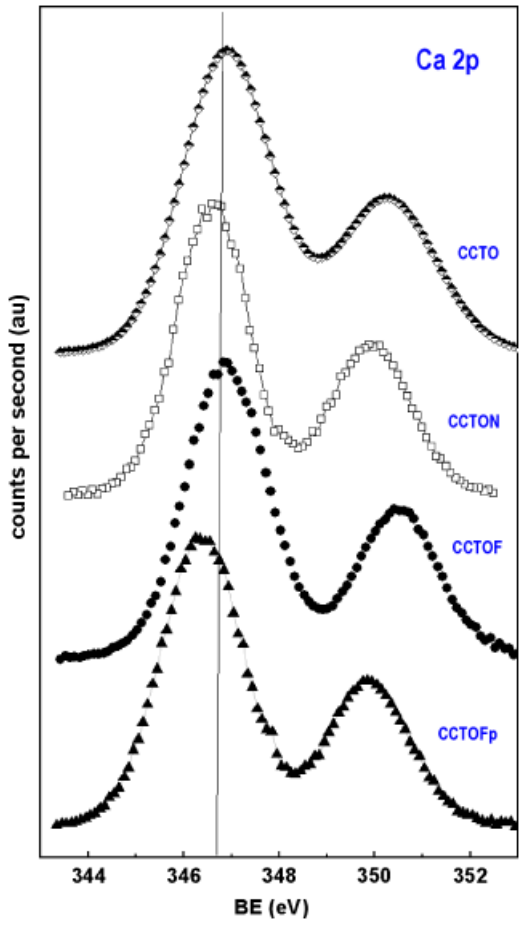

Fig. 6. Photoemission spectroscopy of the Ca $2p_{3/2}$ core level for CCTO-based ceramics.

Figure 6 shows that the oxidation state of Ca $2p_{3/2}$ (346.8 eV) is 2^+, as expected. Nevertheless, the Ca 2*p* of CCTOFp appears carbonated due to air exposure of new surfaces during the milling process. In the case of oxygen, Fig. 7, the O 1*s* peak shows two species: lattice oxygen O_L (529.8 eV) and surface oxygen O_S (531.6 eV). The surface oxygen is associated with surface hydroxyl (or carbonate) groups generated by air exposition and it is more relevant in the samples with larger amounts of reduced copper.

The presence of cations in different oxidation states does change the lattice parameter because, in general, the reduced state shows a larger ionic radius. The ionic radius of Cu^{+1} is 0.96 Å, i.e. ~40% larger than the Cu^{2+} one, 0.69 Å. Changes in the ionic radius of the *A* cation modify the tilting of the TiO_6 octahedron, causing changes in the polarizability of the crystalline lattice. As a consequence, the anomalies observed in the evolution of the lattice parameter must be carefully considered, being not conclusive about the dopant incorporation issue. There is not a clear relationship between the ratio of the reduced/oxidized cation and the high dielectric constant in these samples, and further studies are required to clarify this effect. The balance of the reduced/oxidized state could play an important role during the heating treatment because of the thermodynamic nature of the copper cation, with a trend of being reduced at high temperatures during the sintering step.

The XPS analysis of the powders obtained after milling the ceramic indicates that the chemical states of the layered domains change with the air exposition and allows us to formulate the hypothesis that the twin wall of the layered domains possesses a different composition. Twin walls consist of planar defects that separate domains with uniform but different strains, or electric polarization. Point defects tend to accumulate in the vicinity of twin walls.[32] A significant nanoscale disorder of Cu and Ca cations was observed by quantitative electron diffraction, and extended X-ray absorption fine structure[33] could support this hypothesis. In addition, Kant *et al.*[34] recently found unexplained reflectivity spectra in which each band exhibited two striking crossing points, isosbestic points, which evidence the existence of two components in CCTO. Isosbestic points are usually explained as being due to two components with dynamical conductivity that only depend linearly on density.[35] Isosbestic points have sometimes been identified in transition-metal oxides and were explained in terms of spectral weight transfer driven by strong electronic correlations.[36] In the CCTO system, the existence of two components with a strong electronic coupling has not been considered previously. If the previous hypothesis is consistent enough, the magnetic properties' behavior must reveal concluding evidence.

(3) Magnetic Properties

Figure 8 presents the magnetization versus temperature curves for the different samples. As expected, all of them exhibit paramagnetic behavior at RT, because CCTO is an AFM with a T_N of 25 K. The susceptibility of CCTO at RT is 1.71×10^{-5} emu $\cdot$ (g $\cdot$ Oe)$^{-1}$, in agreement with previously reported values.[16] Surprisingly, substituting 1 wt% of the Ti^{4+} atoms by Fe^{3+} or Nb^{5+} reduces the magnetic susceptibility to a value that is about 40% of that for pure CCTO ($7.12 \cdot 10^{-6}$ emu $\cdot$ (g $\cdot$ Oe)$^{-1}$ for 1 wt% Fe and 6.06×10^{-6} emu $\cdot$ (g $\cdot$ Oe)$^{-1}$ for 1 wt% Nb). This behavior is at odds with the data of Grubbs *et al.*,[7] which showed an enhancement of the magnetic susceptibility when

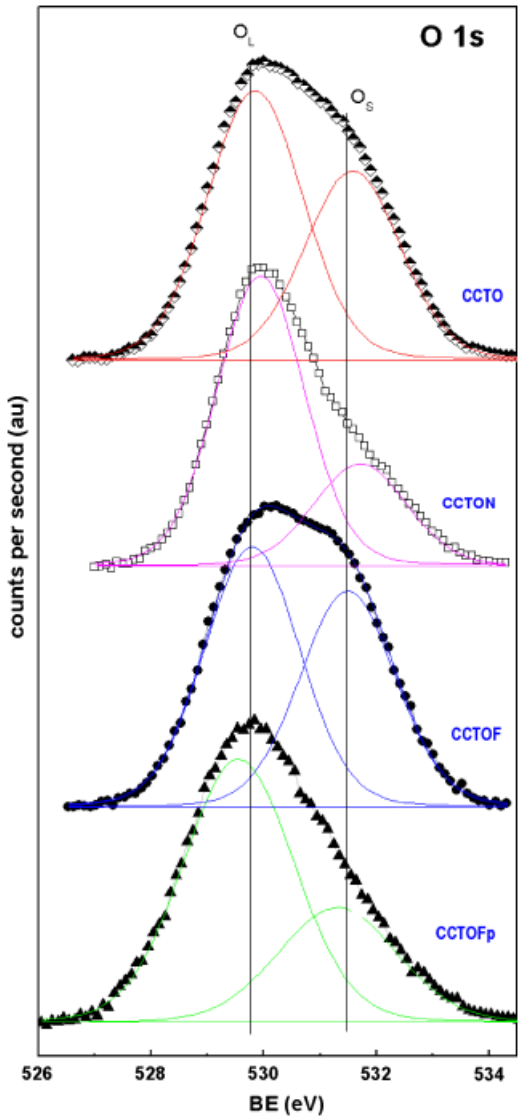

Fig. 7. Photoemission spectroscopy of the O 1*s* core level for CCTO-based ceramics.

doping CCTO. That work also claimed an increase in grain boundary resistivity. Thus, the reduction of the grain boundary resistivity and the decrease of the magnetic susceptibility seem to be a coupled phenomenon.

It is really surprising that substituting just 1 wt% of the B cations can yield such a large modification of the magnetic susceptibility. This change cannot be explained in terms of replacement of the magnetic moment by that of the substituting ion. Actually, Fe is incorporated in CCTO as Fe^{3+} ($3d^5$) and holds a magnetic moment of 5.9 μ_B, while Nb is incorporated as Nb^{5+} ($4s^2$) without a magnetic moment. The small differences in the susceptibility values for doped samples are slightly larger in Fe-doped than in Nb-doped materials and cannot be explained as resulting from the magnetic moment of the doping atom. The difference between the effective magnetic moment and the expected one for a given dopant cation in the crystalline lattice means that the presence of cations modifies the environments and modulates the magnetic moment. Further support for this idea is that doping with 0.3 at.% Fe^{3+} leads to a susceptibility value that is intermediate between those corresponding to the 1 at.% of Fe^{3+} or Nb^{5+}. On the other hand, the large differences with the undoped CCTO cannot be explained in the same terms and must be related to the differences in both grain boundary nature and grain conductivity, as exposed above.

The *M* vs. *T* curves, Fig. 8, exhibit the well-known AFM behavior of CCTO with $T_N \sim 25$ K, for all the samples with the above-shown differences in magnetic susceptibility. In addition, differences in the tail behavior of the magnetic susceptibility below T_N were observed. For AFM materials and $T > T_N$, the dependencies follow the Curie–Weiss law:

$$\chi = \frac{\mu_0 n \mu_{eff}^2}{3K_B(T-\theta)}$$

where μ_{eff} is the magnetic moment of the Cu^{+2} ions and θ the Weiss parameter that accounts for the AFM interactions. Actually, the data for $T > T_N$ can be fitted to this expression with the same value of the Weiss constant for all the samples, $\theta = -32$ K (negative as expected for an AFM material). Neither T_N nor θ changes when doping the material, indicating that the large variation in magnetic susceptibility at 300 K is not associated with changes in the AFM interactions but is ascribed to changes in the value of the individual magnetic moments.

In AFM materials, the magnetic susceptibility below the disorder/order transition at T_N must decrease linearly with temperature,[37] and the value at 0 K must be two-thirds of that at the T_N in a randomly oriented set of moments, as in the case of ceramic materials. In our experiments, the data below T_N are fitted to this expected dependency. Thus, after subtracting the fitted AFM curve to the measured response, a typical paramagnetic-like behavior is revealed (segmented line in Fig. 8). As the Cu^{2+} supports the AFM coupling, the remaining paramagnetic contribution could only be originated by the Ti^{3+} cations. Therefore, fitting the curve to the sum of both contributions allows us to evaluate the magnetic moments ascribed to Cu^{+2} and, to some extent, the magnetic contribution of the Ti cation separately. It is clear that the magnetic response is not decoupled in a crystalline lattice, but this method helps to evaluate the magnetic contribution of cations located in A sites and cations located in B sites. The Ca cations have not been taken into account. The existence of two coupled magnetic contributions to the *M* vs. *T* response contributes to the understanding of the proposed unusual coupling of the AFM Cu superexchange interaction in the CCTO material, which leads to an AFM ordering through the nonmagnetic Ti^{4+}, rather than via the usual oxygen coupling.[15] Table II summarizes those fits. For undoped CCTO, the fit produces 1.7 μB per magnetic site for the contribution that stays paramagnetic in the whole range of temperatures; this value agrees quite well with the expected value for Ti^{3+}. The paramagnetic part, which turns AFM at 25 K, produces a value of 2.13 μB per magnetic site that again agrees quite well with the expected value for Cu^{2+}. On doping with either Fe^{3+} or Nb^{5+}, both values of the magnetic moment decrease, and the T_N of the phase that turns AFM remains basically constant. Nb^{5+} doping decreases the magnetic susceptibility by ~1 μB per Ti site and 0.6 μB per Cu site, while Fe^{3+} doping decreases up to 1.4 μB at both sites.

The good agreement of these fittings confirms that the anomalous magnetic susceptibility below the T_N is due to the presence of Ti^{3+}, as suggested previously.[16] The fact that more reduced Ti cations are found in CCTO seems to correlate with a larger presence of Cu-rich intergranular phase, which means less presence of copper cations in the CCTO lattice. This provokes Ti^{4+} cations to reduce to Ti^{3+} in order to compensate the Cu vacancies. The doping of CCTO produces a reduction of the intergranular Cu-rich phase and thus a decrease of Cu vacancies into the crystalline lattice and a decrease of the Ti^{3+} presence. Because the amount of Cu cations satisfies the composition stoichiometry criteria, their intergrain presence means that there are less Cu cations inside the grains.

The above results clearly evidence the coexistence of two coupled magnetic contributions in the CCTO-based materials. The paramagnetic-like component predominates at low temperatures and could be associated with the observed resistivity increase found below 150 K.[9,22] This experimental fact introduces a new ingredient for understanding the origin of the low-temperature relaxation in the vicinity of AFM coupling, which

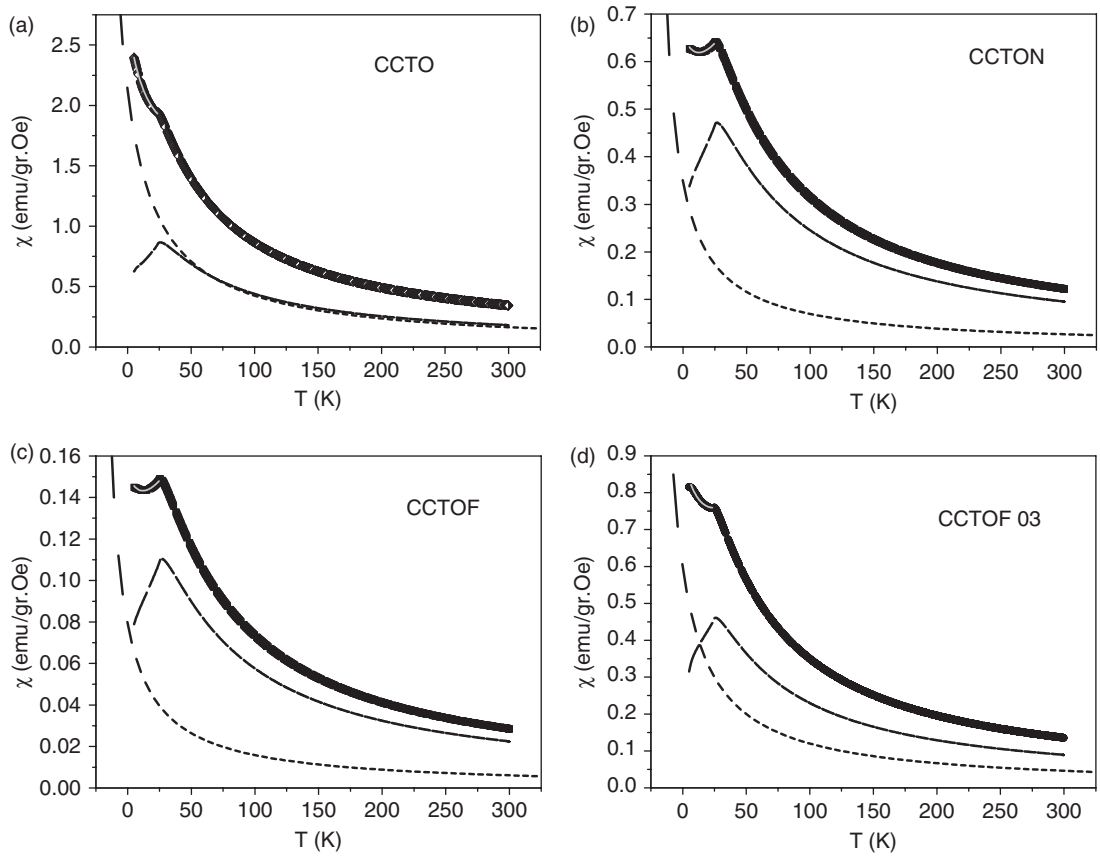

Fig. 8. Fitting results for the magnetic properties of (a) CCTO, (b) CCTON, (c) CCTOF03, and (d) CCTOF. Symbols stand for the experimental results, and the continuous line describes the resulting Curie–Weiss AFM behavior when the magnetic susceptibility was fitted to a linear behavior below T_N. The segmented line is the result of subtracting this fitted Curie–Weiss response from the data.

provokes the grain resistivity to increase and leads to the disappearance of the giant dielectric response. At temperatures >150 K, the paramagnetic-like contribution is reduced, and the increased conductivity allows the appearance of a giant dielectric response, satisfying the IBLC model. For undoped CCTO, the paramagnetic-like behavior is comparable, in magnetic susceptibility, to the AFM response, and the undoped CCTO is thus more resistive in the studied temperature range, and the dielectric constant is moderated.

Moreover, from the comparison between the magnetic results and the values of the dielectric constant measured for the different samples, a direct relationship seems to exist between this constant and the AFM susceptibility. Because the AFM susceptibility is proportional to the quantity of Cu^{2+} atoms in ordered lattice sites, this result points out that the dielectric constant of the material is influenced by the concentration of Cu and vacancies.

These findings show that there is a correlation between the unusual dielectric response and the magnetic properties through the presence of reduced Ti^{3+} cations and the existence of Cu vacancies in the crystalline lattice.

Table II. Magnetic Fitting Parameters

	Paramagnetic contribution (Ti) $\chi_{PM} = \frac{\mu_0 n \mu_{eff}^2}{3K_B(T-\theta)}$; $5 < T < 300$ K		Antiferromagnetic contribution (Cu) $\chi_{AFM} = \frac{\mu_0 n \mu_{eff}^2}{3K_B(T-\theta)}$; $T > T_N$	
Sample	Θ (K)	μ (μ_B)/Ti	Θ (K)	μ (μ_B)/Cu
CCTO	−39.58	1.7	−25	2.13
CCTOF	−29.88	0.32	−25	0.73
CCTON	−30.26	0.68	−25	1.53
CCTOF03	−29.45	0.90	−25	1.48

IV. Conclusions

In summary, our integrated study combining electric, dielectric, and magnetic properties with microstructural and structural characterization reveals the existence of two components in the pseudocubic perovskite.

In this work a grain domain structure, named as layered domains, is observed. The layered domains present different thicknesses in each grain (<80 nm) and thus confer a nanostructure upon the CCTO-based ceramics. Further evidence of the grains layered nature was obtained by milling the ceramic samples, which produced an unusual laminar structure.

The origin of the nanostructured, layered domains has been associated with the presence of different chemical states as Cu^{2+}/Cu^{1+} and Ti^{4+}/Ti^{3+}, the presence of which is determined by XPS. The reduced cations possess larger ionic radii that could originate changes in the octahedron tilting and thus in the polarizability of the system and its properties. Because of previous evidence of nanoscale disorder of Ca and Cu cations,[33] we introduce the hypothesis that the layered domains are formed due to the different polarization states, which is consistent with the trend to accumulate point defects in the twin walls in a perovskite.[32]

The existence of two coupled components is unequivocally determined by analysis of the magnetic properties. It is observed that the M vs. T curve exhibits the typical behavior of an AFM material, plus a low-T paramagnetic-like contribution with different weights. Fitting the sum and both contributions allows us to determine the magnetic moments of the Cu^{2+} and Ti^{3+} cations. The paramagnetic-like contribution affects the resistivity, as lowering the contribution increases the dielectric constant. There

is a correlation between the unusual dielectric response and the magnetic properties through the presence of reduced Ti^{3+} cations and the existence of Cu vacancies in the crystalline lattice.

References

[1]C. C. Homes, T. Vogt, S. M. Shapiro, S. Wakimoto, and A. P. Ramirez, "Optical Response of High-Dielectric-Constant Perovskite-Related Oxide," *Science*, **293**, 673–6 (2001).

[2]T. B. Adams, D. C. Sinclair, and A. R. West, "Giant Barrier Layer Capacitance Effects in $CaCu_3Ti_4O_{12}$ Ceramics," *Adv. Mater.*, **14** [18] 1321–3 (2002).

[3]M. A. Subramanian, D. Li, N. Duan, B. A. Reisnet, and A. W. Sleight, "High Dielectric Constant in $ACu_3Ti_4O_{12}$ and $ACu_3Ti_3FeO_{12}$ Phases," *J. Solid State Chem.*, **151** [2] 323–5 (2000).

[4]T. B. Adams, D. C. Sinclair, and A. R. West, "Decomposition Reactions in $CaCu_3Ti_4O_{12}$ Ceramics," *J. Am. Ceram. Soc.*, **89** [9] 2833–8 (2006).

[5]L. Ni, X. M. Chen, X. Q. Liu, and R. Z. Hou, "Microstructure-Dependent Giant Dielectric Response in $CaCu_3Ti_4O_{12}$ Ceramics," *Solid State Commun.*, **139**, 45–50 (2006).

[6]S. F. Shao, J. L. Zhang, P. Zheng, and C. L. Wang, "Effect of Cu-Stoichiometry on the Dielectric and Electric Properties in $CaCu_3Ti_4O_{12}$ Ceramics," *Solid State Commun.*, **142**, 281–6 (2007).

[7]R. K. Grubbs, E. L. Venturini, P. G. Clem, J. J. Richardson, B. A. Tuttle, and G. A. Samara, "Dielectric and Magnetic Properties of Fe- and Nb-Doped $CaCu_3Ti_4O_{12}$," *Phys. Rev. B*, **72**, 104111 (2005).

[8]P. Leret, J. F. Fernandez, J.de Frutos, and D. Fernandez-Hevia, "Nonlinear I–V Electrical Behaviour of Doped $CaCu_3Ti_4O_{12}$ Ceramics," *J. Eur. Ceram. Soc.*, **27**, 3901–5 (2007).

[9]D. Capsoni, M. Bini, V. Massarotti, G. Chiodelli, M. C. Mozzati, and C. B. Azzoni, "Role of Doping and CuO Segregation in Improving the Giant Permittivity of $CaCu_3Ti_4O_{12}$," *J. Solid State Chem.*, **177**, 4494–500 (2004).

[10]S. H. Hong, D. Y. Kim, H. M. Park, and Y. M. Kim, "Electric and Dielectric Properties of Nb-Doped $CaCu_3Ti_4O_{12}$ Ceramics," *J. Am. Ceram. Soc.*, **90** [7] 2118–21 (2007).

[11]T. T. Fang and C. P. Liu, "Evidence of the Internal Domain for Inducing the Anomalously High Dielectric Constant CCTO," *Chem. Mater.*, **17** [20] 5167–71 (2005).

[12]J. Li, A. W. Sleight, and M. A. Subramanian, "Evidence for Internal Resistive Barriers in a Crystal of the Giant Dielectric Constant Material: $CaCu_3Ti_4O_{12}$," *Solid State Commun.*, **135** [4] 260–2 (2005).

[13]A. Collomb, D. Samaras, B. Bochu, and J. C. Joubert, "Magnetic-Properties and Structure of $CaCu_3Ti_4O_{12}$ with Perovskite Structure," *Phys. Status Solidi A*, **41**, 459–63 (1977).

[14]M. C. Mozzati, C. B. Azzoni, D. Capsoni, M. Bini, and V. Massarotti, "Electron Paramagnetic Resonance of Polycrystalline $CaCu_3Ti_4O_{12}$," *Phys. Condens. Matter.*, **15**, 7365–74 (2003).

[15]C. Lacroix, "Crystallographic and Magnetic-Structures of Materials with Threefold Orbital Degeneracy—Application to $CaCu_3Ti_4O_{12}$," *J. Phys. C*, **13**, 5125–36 (1980).

[16]M. A. Pires, C. Israel, W. Iwamoto, R. R. Urbano, O. Agüero, I. Torriani, C. Rettori, and P. G. Pagliuso, "Role of Oxygen Vacancies in the Magnetic and Dielectric Properties of the High-Dielectric-Constant System $CaCu_3Ti_4O_{12}$: An Electron-Spin Resonance Study," *Phys. Rev. B*, **73**, 224404 (2006).

[17]L. Ni and X. M. Chen, "Dielectric Relaxation and Formation Mechanism of Giant Dielectric Constant $CaCu_3Ti_4O_{12}$ Ceramics," *Appl. Phys. Lett.*, **91**, 122905 (2007).

[18]G. L. Li, Z. Yin, and M. S. Zhang, "First-Principle Study of the Electronic and Magnetic Structures of $CaCu_3Ti_4O_{12}$," *Phys. Lett. A*, **344**, 238–46 (2005).

[19]M. A. Garcia, E. F. Pinel, J de la Venta, A. Quesada, V. Bouzas, J. F. Fernández, J. J. Romero, M. S. Martín González, and J. L. Costa-Krämer, "Sources of Experimental Error in the Observation of Nanoscale Magnetism," *J. Appl. Phys.*, **105**, 013925 (2009).

[20]D. C. Sinclair, T. B. Adams, F. D. Morrison, and A. R. West, "$CaCu_3Ti_4O_{12}$: One-Step Internal Barrier Layer Capacitor," *Appl. Phys. Lett.*, **80** [12] 2153–5 (2002).

[21]G. Chiodelli, V. Massarotti, D. Capsoni, M. Bini, C. B. Azzoni, M. C. Mozzati, and P. Lupotto, "Electrical and Dielectrical Properties of Pure and Doped $CaCu_3Ti_4O_{12}$ Perovskite Materials," *Solid State Commun.*, **132**, 241–6 (2004).

[22]D. L. Sun, A. Y. Wu, and S. T. Yin, "Structure, Properties, and Impedance Spectroscopy of $CaCu_3Ti_4O_{12}$ Ceramics Prepared by Sol–Gel Process," *J. Am. Ceram. Soc.*, **91** [1] 169–73 (2008).

[23]L. Marchin, S. Guillemet-Fritsch, B. Durand, A. A. Levchenko, A. Navarotsky, and T. Lebey, "Grain Growth-Controlled Giant Permittivity in Soft Chemistry $CaCu_3Ti_4O_{12}$ Ceramics," *J. Am. Ceram. Soc.*, **91** [2] 485–9 (2008).

[24]G. Z. Zang, J. L. Zhang, P. Zheng, J. F. Wang, and C. L. Wang, "Grain Boundary Effect on the Dielectric Properties of $CaCu_3Ti_4O_{12}$ Ceramics," *J. Phys. D: Appl. Phys.*, **38**, 1824–7 (2005).

[25]P. R. Bueno, R. Tararan, R. Parra, E. Joanni, M. A. Ramirez, W. C. Ribeiro, E. Longo, and J. A. Varela, "A Polaronic Stacking Fault Defect Model for $CaCu_3Ti_4O_{12}$ Material: An Approach for the Origin of the Huge Dielectric Constant and Semiconducting Coexistent Features," *J. Phys. D: Appl. Phys.*, **42**, 055404 (2009).

[26]L. Wu, Y. Zhu, S. Park, S. Shapiro, G. Shirane, and J. Tafto, "Defect Structure of the High-Dielectric-Constant Perovskite $CaCu_3Ti_4O_{12}$," *Phys. Rev. B*, **71**, 014118 (2005).

[27]R. E. Chinn, *Ceramography: Preparation and Analysis of Ceramic Microstructure*. ASM International and the American Ceramic Society, Westerville, OH, USA, 2002.

[28]S. S. Chung, "Lattice Distortion and Polarization Switching in Calcium Copper Titanate," *Appl. Phys. Lett.*, **87**, 052901 (2005).

[29]H. A. Bullen and S. J. Garret, "TiO_2 Nanoparticle Arrays Prepared Using a Nanosphere Lithography Technique," *Nano Lett.*, **2**, 739–45 (2002).

[30]I. Jacyna-Onyszkiewicz, M. Zimpel, M. A. Obolensky, Y. B. Poltoracky, S. Starodub, and S. Robaszkiewicz, "Transport Properties and Electronic Structure of New Rare Earth-Copper Chalcogenides," *Phys. B: Condens. Matter*, **239** [2–3] 283–92 (1997).

[31]A. F. Carley, M. W. Roberts, J. S. Lees, and R. J. D. Tilley, "X-Ray Photoelectron Spectroscopic Study of the High-Tc Superconductor $YBa_2Cu_3O_{7-X}$ Evidence for Cu^{3+} and Surface Oxygen Excess," *J. Chem. Soc. Faraday Trans.*, **86** [18] 3129–34 (1990).

[32]D. Shilo, G. Ravichandran, and K. Bhattacharya, "Investigation of Twin-Wall Structure at the Nanometre Scale Using Atomic Force Microscopy," *Nat. Mater.*, **3** [7] 453–7 (2004).

[33]Y. Zhu, J. C. Zheng, L. Wu, A. I. Frenkel, J. Hanson, P. Northrup, and W. Ku, "Nanoscale Disorder in $CaCu_3Ti_4O_{12}$: A New Route to the Enhanced Dielectric Response," *Phys. Rev. Lett.*, **99** [3] 037602 (2007).

[34]C. Kant, T. Rudolf, S. Krohns, P. Lukenheimer, S. G. Ebbinghaus, and A. Loidl, "Broadband Dielectric Response of $CaCu_3Ti_4O_{12}$: From dc to the Electronic Transition Regime," *Phys. Rev. B*, **77**, 045131 (2008).

[35]M. Eckstein, M. Kollar, and D. Vollhardt, "Isosbestic Points in the Spectral Function of Correlated Electrons," *J. Low Temp. Phys.*, **147** [3–4] 279–93 (2007).

[36]Y. Okimoto, T. Katsufuji, Y. Okada, T. Arima, and Y. Tokura, "Optical-Spectra in $(La,Y)TiO_3$—Variation of Mott-Hubbard Gap Features with Change of Electron Correlation and Band Filling," *Phys. Rev. B*, **51** [15] 9581–8 (1995).

[37]K. H. J. Buschow and F. R. de Boer, *Physics of Magnetism and Magnetic Materials*, p. 26. Kluwer Academic Press, 2004. □